Chemical Engineering Journal 149 (2009) 196–206

Contents lists available at ScienceDirect

Chemical Engineering Journal

journal homepage: www.elsevier.com/locate/cej

Adsorption of fluoride by hydrous iron(III)–tin(IV) bimetal mixed oxide from the aqueous solutions

Krishna Biswas, Kaushik Gupta, Uday Chand Ghosh*

Department of Chemistry, Presidency College, 86/1 College Street, Kolkata 700073, India

ARTICLE INFO

Article history:
Received 2 March 2008
Received in revised form
17 September 2008
Accepted 25 September 2008

Keywords:
Adsorption
Fluoride
Kinetics
Iron(III)–tin(IV) mixed oxide
Thermodynamics

ABSTRACT

The synthetic iron(III)–tin(IV) mixed oxide (HITMO) has been characterized by the FTIR, XRD and SEM image analyses. The mixed oxide is found hydrated and amorphous with irregular surface morphology. The relevant parameters studied for fluoride removal by using HITMO are the effects of pH, contact time, and equilibrium. The fluoride adsorption capacity is nearly constant in the pH range 5.0–7.5. The pseudo-second order equation explains the kinetic data well and, the overall rate is multi-stage controlled. The Langmuir isotherm describes the equilibrium data well and gives high Langmuir capacity (~10.50 mg g^{-1}) value. The mean adsorption energy (9.05 kJ mol^{-1}) computed from the Dubinin–Redushkevich isotherm suggests the ion exchange mechanism for fluoride adsorption. The evaluated change of enthalpy (ΔH^0), entropy (ΔS^0) and free energy (ΔG^0) of adsorption values indicates the endothermic and non-spontaneous nature of the present reaction. Excepting bicarbonate, other common ions show no adverse effect on fluoride removal. The regeneration (~75%) of fluoride-rich (10.0 mg g^{-1}) material is possible by a solution of pH 13.0. Two gram HITMO per litre of the fluoride-doped (2.97 mg L^{-1}) natural water reduces fluoride level below 1.5 mg L^{-1}.

1. Introduction

The optimum concentration of fluoride ion in drinking water is ranged in 0.5–1.0 mg L^{-1} for the good health of teeth and bones of mammals. However, long-term intake of excess fluoride through food and drinks might be the cause of dental and skeletal fluorosis. Ground water, which is the main source of drinking water in rural areas of underdeveloped countries like India, if contaminated with excess fluoride ion (>1.5 mg L^{-1}) is a great concern to the public health. India is among 23 nations in the world, where fluorosis is found to be prevalent. It had been estimated that about 62 million people in 19 states of India are affected with different forms of fluorosis, which include dental and skeletal fluorosis [1]. The high level of fluoride ion in groundwater (>1.5 mg F^- L^{-1}) is due to some geochemical reactions [2] in sub-surface soil. Depending on the geological formation, fluorite and fluoroapatite minerals are hosted in the vein of all most all rocks in sub-surface soil. The bicarbonate-rich water from the topsoil when percolates through the mineral bed undergoes water-mineral interaction and, releases fluoride due to some chemical reactions [2] under the geophysical conditions. The released fluoride, thus, mobilizes to the ground water unless any other natural phenomena play any significant role for reducing fluoride level from that percolated water.

Traditional treatment methods such as chemical precipitation, membrane process, electro deposition, surface adsorption and ion exchange were reported to use for fluoride removal from water. The surface adsorption, among them, has been found to be the most important one for the third world countries like India for easy operation, affordable cost and water quality. Different adsorbent materials such as natural, synthetic, and biomass had been investigated for the adsorptive removal of fluoride from the aqueous solution [3–35] in last few years. Among them, synthetic and hydrous oxides such as iron(III) oxide [32], zirconium(IV) oxide [33], iron(III)–zirconium(IV) hybrid oxide [34] and iron(III)–aluminum(III) mixed oxide [35] had been used in our laboratory for the fluoride removal studies. Iron(III) oxide, highly abundant in the earth crust, is one of the natural water purifier. However, the synthetic hydrous iron(III) oxide [32] showed low adsorption affinity for the hard fluoride ion from the aqueous solution. Aiming to increase the fluoride adsorption capacity of iron(III) oxide from the contaminated water, we have been incorporating metal ions of high ionic potential (hard metal ion) into the lattice of aforesaid metal oxide for the systematic use of fluoride adsorption from the aqueous solution. With this objectives, tin(IV), a cation with high positive charge, has been incorporated into the lattice structure of iron(III) oxide and used as an adsorbent for the removal of the hard fluoride ion from the aqueous phase.

* Corresponding author. Tel.: +91 33 2241 3893; fax: +91 33 2241 3893.
E-mail address: ucghosh@yahoo.co.in (U.C. Ghosh).

1385-8947/$ – see front matter © 2008 Elsevier B.V. All rights reserved.
doi:10.1016/j.cej.2008.09.047

Nomenclature

A	temperature-independent factor (g mg^{-1} min^{-1})
b	equilibrium adsorption constant (L mg^{-1})
C	intra-particle (pore) diffusion constant
C_e	equilibrium fluoride (mg L^{-1}) concentration in solution
C_i	initial fluoride concentration (mg L^{-1}) in solution when time, $t = 0$
C_L	concentration of solute in liquid phase (mg L^{-1}) at $t = 0$
C_s	concentration of solute in solid phase (mg g^{-1}) at equilibrium time, t
C_t	concentration of fluoride solution (mg L^{-1}) at a time (t, min)
D_F	film diffusion coefficient (cm^2 s^{-1})
D_P	pore diffusion coefficient (cm^2 s^{-1})
D–R	Dubinin–Radushkevick equation
E_a	activation energy of adsorption (kJ mol^{-1})
E_{DR}	mean free energy of adsorption (kJ mol^{-1})
ΔG^0	standard Gibbs free energy change (kJ mol^{-1})
h_0	initial adsorption rate (mg g^{-1} time^{-1})
ΔH^0	standard enthalpy change (kJ mol^{-1})
K_c	equilibrium constant
K_F	Freundlich constant (mg$^{1-1/n}$ L$^{1/n}$ g^{-1})
k_{id}	intra-particle (pore) diffusion rate constant (mg g^{-1} time$^{-0.5}$)
k_1	pseudo-first order rate constant (time^{-1})
k_2	pseudo-second order rate constant (g mg^{-1} min^{-1})
m	mass of solid (adsorbent) added (g)
n	Freundlich constant (dimensionless)
q_e	Equilibrium adsorption capacity (mg g^{-1})
q_m	adsorption capacity (mol kg^{-1})
q_t	adsorption capacity (mg g^{-1}) at a time (t, min)
R	universal gas constant (8.314 J mol^{-1} K^{-1})
r^2	linear regression coefficient
r_0	mean radius of adsorbent particles (cm) (assumed spherical)
ΔS^0	standard entropy change (J mol^{-1} K^{-1})
T	absolute temperature (K)
t	time (min)
$t_{1/2}$	time for 50% adsorption (s)
V	solution volume (L)
ZPC	zero point charge

Greek symbols

β	constant of D–R isotherm equation (mol^2 kJ^{-2})
ε	Polanyi potential
θ	Langmuir monolayer adsorption capacity (mg g^{-1})
∂	film thickness (cm)

Thus, we report herein the synthesis and characterization of hydrous iron(III)–tin(IV) bimetal mixed oxide (HITMO), and application of the mixed oxide (HITMO) for adsorption of fluoride from the aqueous solution.

2. Materials and methods

2.1. Synthesis of HITMO

The synthesis of HITMO was made by hydrolyzing well-stirred 0.1 M $FeCl_3$ (in 0.1 M HCl) solution with 0.1 M Na_2SnO_3 (in 0.2 M NaOH) at room temperature followed by addition of 0.1 M NaOH to reach the supernatant liquid pH 5.3 (±0.2). The brown gel precipitate aged for three overnight was filtered, washed with deionized water and dried at 70 °C in an air oven. The dried hot product when treated with cold water was broken to small particles. It was sieved (B. S. Sieve) for the fraction between 50 and 100 mesh (particle size: 0.14–0.29 mm), and homogenized to a definite pH for working. The HITMO material was heat-treated at 250 °C for an hour into a muffle furnace and used for the experiments.

2.2. Chemicals

Sodium fluoride (AR, BDH) was used to prepare a stock solution of fluoride (1000 mg L^{-1}). Sodium 2-(para sulfo phenylazo)-1,8-dihydroxy-3,6-naphthalene disulfonate (SPADNS) and zirconium oxychloride used for fluoride estimation [36] were purchased from E. Merck India Ltd., Mumbai, India. All other chemicals used were analytical/guaranteed reagent.

2.3. Instruments

The UV–vis spectrophotometer (Model U-3210) made of Hitachi (Japan) was used for colorimetric analysis of fluoride. An ELICO-made pH meter (Model LI-127) was used for pH analysis. The PerkinElmer-RXIFT spectrophotometer was used for the Föurier Transformed Infrared (FTIR) spectrum. Phillips X-ray diffractometer was used for the powder X-ray diffraction (XRD) analysis of the mixed oxide. Thermogravimatric (TG) and differential thermal (DT) analyzes were made by the Setaram Analyzer in argon gas atmosphere at a heating rate 20 °C min^{-1} over a temperature range up to 900 °C. The BET surface area was analyzed by N_2 gas adsorption at 77 K using Quantachrome (Model Nova 1000e series, USA) surface analyzer. The Scanning Electron Microscope (JSM-5200) was used for the scanning electron microscopic (SEM) image. The zero point surface charge pH (pH_{zpc}) value of the synthetic HITMO was estimated by the method as described by Babic et al. [37].

2.4. Adsorption experiments

Fifty milliliters of the fluoride solution was taken in a 250 mL PVC bottle and 0.1 g of the adsorbent material was added into it. The reaction mixture was placed in a thermostat shaker, and agitated (300 ± 5 rpm). The effect of solution pH ranged in 3.0–10.0 on fluoride removal was studied by adjusting solution pH with 0.1 M HCl or 0.1 M NaOH. The time dependent adsorption reaction was conducted separately with fluoride solution (pH 6.4 ± 0.2) of concentrations 10.0, 15.0 and 25.0 mg L^{-1} as well as at four different temperatures (±1.6 K) [283, 298, 313 and 328 K]. The vessel with reaction mixture was taken out from the shaker, and filtered as soon as possible using 0.45-μm membrane filters. The clear filtrates were analyzed for remaining fluoride concentration with UV–vis spectrophotometer using SPADNS–$ZrOCl_2$ reagent [36]. The adsorption capacity at any time, t (q_t, mg g^{-1}) was calculated using the relation (Eq. (1)):

$$q_t = \frac{V(C_i - C_t)}{m} \quad (1)$$

The significance of the symbols used in Eq. (1) has been given in nomenclature.

The isotherm experiment was also conducted as above but agitation was continued for 2 h for the equilibrium. The fluoride solution (pH 6.4 ± 0.2) of concentration (mg L^{-1}) ranged in 10.0–50.0 was used for the equilibrium test. The residual fluoride concentration (C_e, mg L^{-1}) was analyzed in equilibrated solution and, equilibrium capacity (q_e, mg g^{-1}) was calculated using above equation (Eq. (1)) putting C_e in place of C_t.

2.5. Fluoride removal from natural water

Ground water sample was collected from a tube well (depth: 50 m) of College Square area, Kolkata 700073 (India). The parameters analyzed (in mg L^{-1} except pH) for the composition of the water sample were: pH 7.75, total hardness (as $CaCO_3$) 704, total alkalinity 727, Ca^{2+} 221.24, Mg^{2+} 174.38, Fe (total) 0.05, TDS 1201, Cl^- 357.7, F^- 0.35 and As(total) 0.03. To this water sample, a measured volume of standard fluoride solution was added from outside to increase the concentration to 3.0 mg L^{-1}. The concentration of fluoride in the spiked water sample was re-analyzed and found to be 2.97 mg L^{-1}, and used for the treatment with varying the adsorbent (HITMO) dose from 0.5 to 3.0 g L^{-1} of the sample by the batch process. Here, the solid material, HITMO, of a definite amount (in g) was added in separate six PVC containers in each of which one liter of the fluoride added (2.97 mg L^{-1}) water sample was taken, and mixed well by a digital mechanical stirrer (speed: 1000 rpm) for 2 h. The filtered water from the solid adsorbent particles was analyzed for the residual fluoride [36].

3. Results and discussion

3.1. Characterization of the mixed oxide

The FTIR spectra (Fig. 1) of synthetic (A) hydrous ferric oxide (HFO) (B) HITMO and (C) hydrous stannic oxide (HSO) show broad absorption peaks ranged in the wave number (cm^{-1}) 3000–3750 with maximum pointed, respectively, at 3401.9, 3397.2, and 3429.6. These peaks are for the stretching vibration mode of lattice water and hydroxide groups. The bands found ranged between the wave number (cm^{-1}) 1624 and 1637 are for the OH bending vibration mode of water molecules. The broad peaks at 969.8, 842.7, and 954.4 cm^{-1}, respectively, for HITMO (B), HFO (A) and HSO (C) are for the bending vibration mode for bridging OH group. The peak obtained for HITMO at lower wave number (528.0 cm^{-1}) to that of HFO (682.6 cm^{-1}) and HSO (564.9 cm^{-1}) has indicated the presence of some interactions between iron(III) and tin(IV) presumably through oxygen or hydroxide bridge. Thus, the synthetic HITMO has assumed to be a hydrous bimetal composite mixture.

The X-ray diffraction (XRD) pattern (graph omitted) of HITMO has suggested amorphous nature of the product. The TG spectrum of HITMO shows (figure omitted) 21.1% and 1.32% loss of weight in the drying temperature (°C) range, respectively, at 30°–130° and >130°–900°. The weight loss (21.1%) obtained up to 130 °C is attributed to the physically adsorbed water molecules, and is the moisture content of HITMO. The absence of exothermic peak in DT spectrum (graph omitted) has indicated that the material does not undergo polymerization or crystallization when dried up to 900 °C. The surface area ($m^2\ g^{-1}$) determined for HITMO (127.0) has been found to be lesser than either the HFO (165.6) or the HSO (140.8), and that is presumably due to the diffusion of tin(IV) oxide into the lattice structure of the HFO. The analyzed iron to tin mole ratio and pH_{zpc} of the mixed oxide composite obtained are 1:1 and 6.5 (±0.3), respectively. The analysis of SEM images (Fig. 2) of HITMO shows the irregularity in surface morphology (image-a: 35 times magnification), and agglomeration of amorphous nano-powder (image-b: 1000 times magnification) material.

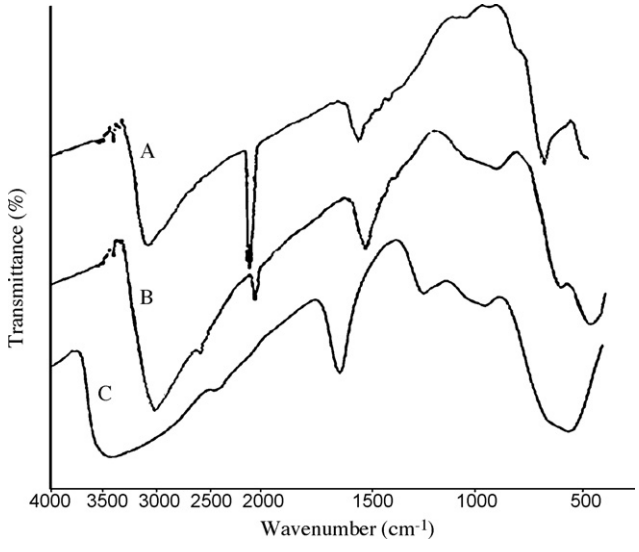

Fig. 1. The Fourier Transformed Infrared (FTIR) spectra of (A) hydrous ferric oxide (HFO) (B) hydrous iron(III)–tin(IV) bimetallic mixed oxide (HITMO) and (C) hydrous stannic oxide (HSO).

3.2. Effect of pH

Fig. 3 shows the influence of initial solution pH (pH_i) on fluoride removal by HITMO. The results have showed (Fig. 3) that the fluoride adsorption capacity (mg g^{-1}) declines sharply with increasing pH_i from 3.0 to 5.0, and remains nearly constant up to pH_i 7.5 and that declines again with increasing pH_i from 7.5 to 10.0. The high adsorption capacity found at pH_i 3.0 is presumably due to the electrostatic attraction (R1) of fluoride by the surface positive charge or ligand/anion-exchange (R2) reaction of fluoride with surface hydroxyl group of the solid adsorbent (pH_{zpc} 6.5 ± 0.3). The decrease in adsorption capacity with increasing pH_i from 3.0 to 5.0 is due to the decrease of surface positive charge density or ion

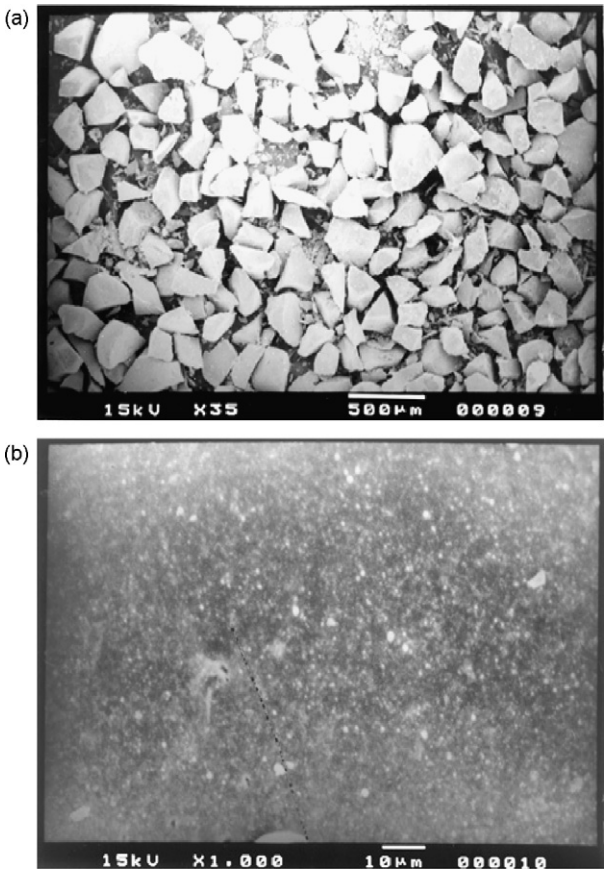

Fig. 2. The scanning electron microscopic (SEM) image of HITMO with (a) 35 times (b) 1000 times magnification.

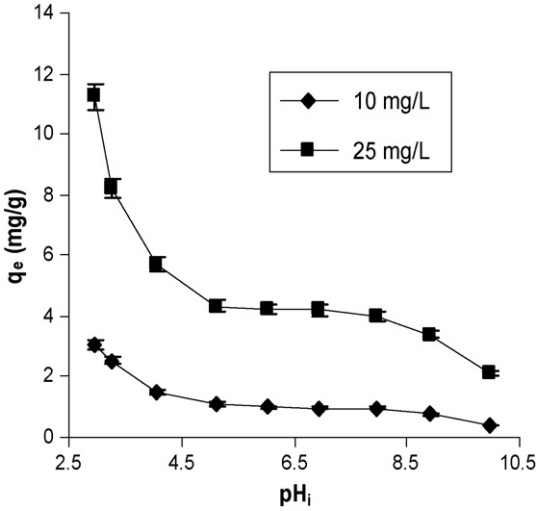

Fig. 3. The effect of initial pH (pH_i) on fluoride adsorption by HITMO at 303 (±1.6) K.

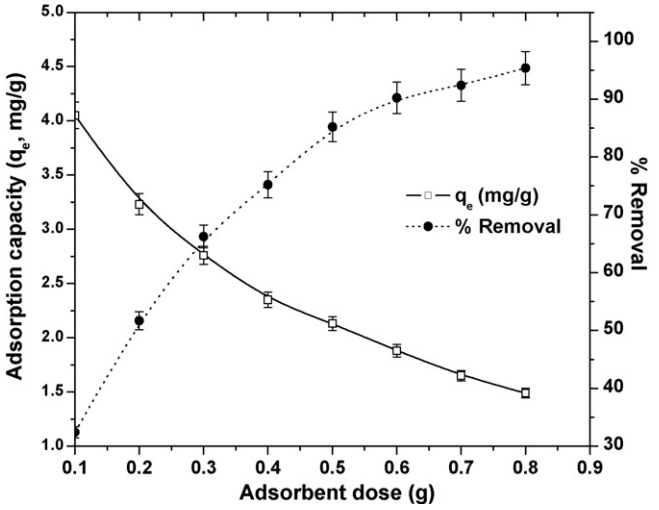

Fig. 4. The effect of HITMO dose on fluoride removal from 50 mL of 25.0 mg L^{-1} fluoride solution at 303 (±1.6) K and at pH 6.40 (±0.2).

exchange capacity of the solid. The capacity remains nearly unaltered at pH_i ranged in >5.0 to <7.5, which is presumably due to the neutral or near neutral surface of the solid.

$$MOH_{(S)} + H_3O^+ + F^- \rightarrow MOH_2^+ \cdots F^-_{(S)} + H_2O \quad (R1)$$

$$MOH_{(S)} + H_3O^+ + F^- \rightarrow M^+ \cdots F^-_{(S)} + 2H_2O \quad (R2)$$

$MOH_{(s)}$ stands for the solid material. The columbic or anion-exchange type fluoride adsorption mechanism ((R1) or (R2)) as suggested is consistent well with the observed increase of the equilibrium solution pH.

The adsorption reaction that has taken place at pH_i ranged in >5.0 to <7.5 may be described by the following ligand/anion-exchange type reaction (R3). This agrees well with the observed notable increase of equilibrium solution pH.

$$M\text{–}OH_{(S)} + F^-_{(aq)} \rightarrow M^+ \cdots F^-_{(S)} + OH^-_{(aq)} \quad (R3)$$

The surface of the solid should be negative at $pH > pH_{zpc}$ and, the fluoride adsorption capacity thus declines due to the columbic repulsion of like charges between the solute in solution and the solid surface. The low adsorption capacity obtained at $pH_i > 7.5$ is due to the adsorption of fluoride competing with hydroxyl ion at the secondary adsorption sphere (R4) where the Na^+ (available in solution) is at the first adsorption sphere of the solid adsorbent.

$$MOH_{(S)} + Na^+_{(aq)} + F^-_{(aq)} + OH^- \rightarrow MO^- \cdots Na^+ \cdots F^- + H_2O \quad (R4)$$

The adsorption reaction (R4) as suggested agrees well with the decrease of equilibrium solution pH.

3.3. Effect of HITMO dose

Fig. 4 shows the effect of HITMO dose (in g) on the fluoride removal at pH 6.4 (±0.2). It has been found that the fluoride removal percentage increases from 32.40 to 95.36 when the dose of HITMO had been increased from 0.10 to 0.80 g, and, that increases to the negligible extent even the increase of the adsorbent dose over 0.80 g. Furthermore, the adsorption capacity (q_e, mg g^{-1}) value has decreased for a fixed fluoride concentration (25.0 mg L^{-1}) with the increase of dose. This agrees well with the increase of solid dose for a fixed solute load, and surface sites heterogeneity of the adsorbent. According to surface site heterogeneity model, the surface is composed of sites with a spectrum of binding energies. At the low adsorbent dose, all types of sites are entirely exposed and the adsorption on the surface is saturated faster showing a higher q_e value. But at higher adsorbent dose, the availability of higher energy sites decreases with a large fraction of lower energy sites occupied, resulting in a lower q_e value [16,23].

3.4. Kinetic modeling

3.4.1. Effect of concentration

Fig. 5 shows the plots of kinetic data on fluoride adsorption at 303 (±1.6) K and at pH 6.4 (±0.2) by the HITMO surface. The fluoride adsorption has been found to be rapid in the first 30 min of contact where ~90% of the equilibrium adsorbed amount has taken place by the adsorbent. The remaining ~10% adsorption has taken place by 90 min more contact time. The time required in reaching equilibrium has increased with increasing solute concentration and that has been found to be 120 min for the highest concentration studied. The initial rapid adsorption is presumably due to ion exchange with surface hydroxyl ions of the adsorbent and, the later stage slow adsorption is for the gradual uptake of fluoride at the inner surface.

The time dependent adsorption data shown (Fig. 5) have been analyzed using the linear form of the kinetic equations (Eqs. (2)–(4))

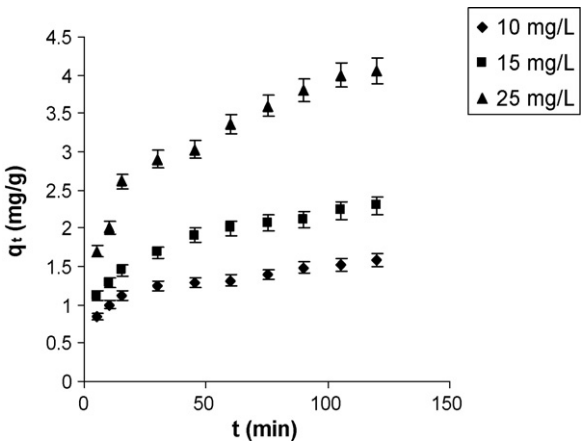

Fig. 5. Effect of initial concentration on adsorption kinetics of fluoride by HITMO ($T = 303 \pm 1.6$) K and at pH 6.40 (±0.2).

Table 1
The kinetic parameters obtained for fluoride adsorption on HITMO at different concentrations [temperature: 303 (±1.6) K] and pH 6.4 (±0.2).

Kinetic equations	Parameters	Fluoride concentration (mg L^{-1})		
		10	15	25
Pseudo-second order	k_2 (g mg^{-1} min^{-1}) × 10^{-2}	7.41	4.08	1.70
	q_e (mg g^{-1})	1.62	2.41	4.37
	r^2	0.993	0.995	0.990
	h_0 (mg g^{-1} min^{-1})	0.200	0.238	0.333
Pseudo-first order	$k_1 \times 10^{-2}$ (min^{-1})	2.18	2.49	3.01
	q_e (mg g^{-1})	0.75	1.31	3.03
	r^2	0.954	0.967	0.900
Intra-particle diffusion	k_{id} (g mg^{-1} $min^{0.5}$) × 10^{-1}	1.12	1.76	3.25
	r^2	0.813	0.880	0.917

[38–40] as shown below:

$$\text{Pseudo-first order}: log(q_e - q_t) = \log q_e - \frac{k_1 t}{2.303} \quad (2)$$

$$\text{Pseudo-second order}: \frac{t}{q_t} = \frac{1}{k_2 q_e^2} + \frac{t}{q_e} \quad (3)$$

$$\text{Intra particle diffusion}: q_t = k_{id} t^{1/2} + C \quad (4)$$

The significance of the symbols present in the above equations (Eqs. (2)–(4)) has been given in the nomenclature.

The related kinetic equation parameters evaluated by the calculation from the slopes and intercepts of the linear plots (best-fit plots given), are shown in Table 1. The pseudo-first order kinetic equation (Eq. (2)) has described the kinetic data fairly well (r^2 = ~0.900–0.970) but less well than the pseudo-second order kinetic equation (Eq. (3)) (r^2 = 0.990–0.995). The pseudo-second order rate constant (k_2), adsorption affinity ($h_0 = k_2 q_e^2$) and equilibrium capacity (q_e) evaluated (Table 1) by calculation from the slopes and intercepts data of the plots (Fig. 6) have showed the decrease of pseudo-second order rate constant (k_2) values and the increase of h_0 and q_e values with increasing initial fluoride concentration. Thus, the rate of adsorption decreases with increasing solute concentrations, which is similar to the results that had been reported using some different system by some other workers [41–43]. To evaluate the actual rate-limiting step for the present system, the data (Fig. 5) have also been analyzed by the intra-particle diffusion kinetic equation (Eq. (4)). Fig. 7 shows the plots of mass of fluoride adsorbed per unit mass of HITMO (q_t, mg g^{-1}) versus square root of contact time ($t^{0.5}$, $min^{0.5}$). The data points appeared in Fig. 7 could be joined by the two straight lines those indicate the first linear portion for the macro-pore diffusion and the second depicting the micro-pore diffusion [13,27,44–47]. The extrapolation of the first linear portion of the plots (excluding the point at zero) back to the axis showing q_t (mg g^{-1}) gives positive intercept which provide the idea about boundary layer thickness (C), and to be found the boundary layer thickness increases with concentration. The extrapolation of first linear portion of plots (Fig. 7) should not pass through the origin, so the adsorption rate for the present case is not solely pore diffusion controlled. If the data points shown in Fig. 7 be connected from zero, the initial sharp line showing variation of q_t versus $t^{0.5}$ values in Fig. 7 should attribute to the boundary layer diffusion effect or external mass transfer effect [13,27,44–47]. Thus, the adsorption data has indicated that the fluoride removal from aqueous phase by the studied mixed oxide is rather complex process involving both boundary layer diffusion and intra-particle diffusion. The values of k_{id} (average pore diffusion rate constant, mg g^{-1} $min^{-0.5}$) are found to increase with increasing concentration (Table 1) indicating the higher pore sorption possibility of the solute on to the adsorbent at room temperature. However, the pore diffusion coefficient (D_P, cm^2 s^{-1}) and film diffusion coefficient (D_F, cm^2 s^{-1}) have been calculated using the following standard relations (Eqs. (5) and (6)) [48,49].

$$D_P = \frac{0.03 r_0^2}{t_{1/2}} \quad (5)$$

$$D_F = \frac{0.23 \times r_0 \times \partial \times C_s}{t_{1/2} \times C_L} \quad (6)$$

where the film thickness (∂) is 0.001 cm [48], and the significance of the terms present in the Eqs. (5) and (6) has given in the nomenclature. Here, $t_{1/2}$ (the time for 50% adsorption) values used for calculation are evaluated from the relation, $t_{1/2} = 1/(q_e k_2)$, where k_2 and q_e have their same meaning mentioned elsewhere. It is known [48] that if the D_p values be ranged in 10^{-11} to 10^{-13} cm^2 s^{-1},

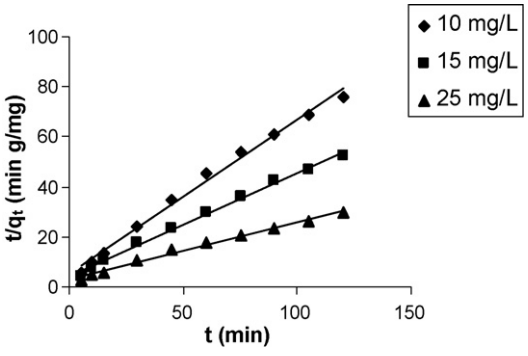

Fig. 6. The pseudo-second order plots related to the effect of initial concentration on adsorption kinetics of fluoride by HITMO (T = 303 (±1.6) K and at pH 6.40 (±0.2).

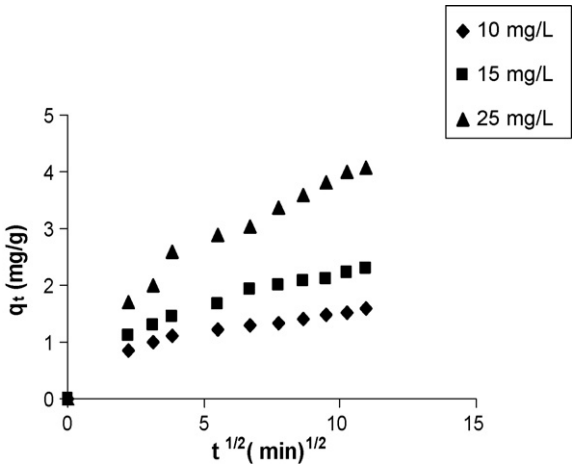

Fig. 7. The intra-particle diffusion plots related to the effect of initial concentration on adsorption kinetics of fluoride by HITMO (T = 303 (±1.6) K and at pH 6.40 (±0.2).

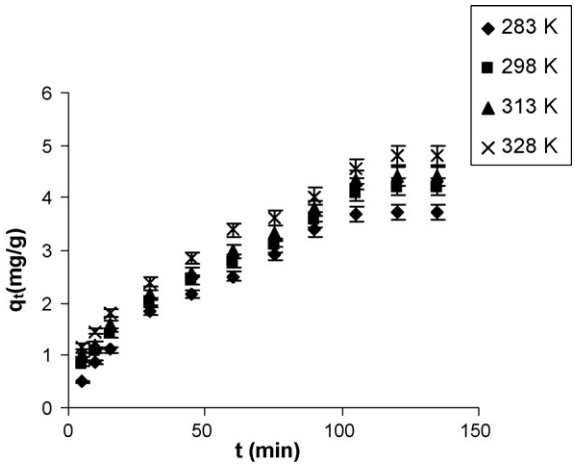

Fig. 8. Effect of temperature on adsorption kinetics of fluoride by HITMO (C_i = 25 mg L^{-1} and pH 6.40 (±0.2).

the pore diffusion is the rate limiting and if the D_F values be ranged in 10^{-6} to 10^{-8} cm^2 s^{-1}, the boundary layer (film) diffusion is the rate-limiting step. The D_p and D_F values (cm^2 s^{-1}) calculated, respectively, for the present case have been found in the range $(4.49–7.27) \times 10^{-9}$ and $(5.48–8.2) \times 10^{-10}$ for the studied concentrations of fluoride. It has been found that the values of either D_p or D_F are not laid in the appropriate range, which indicate the rate-limiting step is multi-stage controlled phenomena for the present case.

3.4.2. Effect of temperature

Fig. 8 shows the fluoride adsorption kinetic data obtained at studied four different temperatures and at pH 6.4 (±0.2) on HITMO surface. The data have also been analyzed by using the kinetic equations (Eqs. (2)–(4)) [38–40] and, the parameters calculated from the slopes and intercepts of the linear plots are given in Table 2. The pseudo-first order kinetic equation (Eq. (2)) has described (plots not shown) the present adsorption kinetic data much less well (r^2 = 0.799–0.931). In contrast, the pseudo-second order equation (Eq. (3)) has described the data of Fig. 8 quite well (r^2 = 0.958–0.983) (Fig. 9). The equilibrium adsorption capacity (q_e, mg g^{-1}) and the initial adsorption rate ($h_0 = k_2 q_e^2$) calculated from the linear plots (Fig. 9) according to Eq. (3) have increased, respectively, from 5.29 to 5.84 and 0.095 to 0.167 with the increase of temperature from 283 (±1.6) to 328 (±1.6) K. So, from the above q_e and h_0 values (Table 2), the endothermic nature of the adsorption process has been indicated. In addition, the pseudo-second order rate constant ($k_2 \times 10^{-3}$, g mg^{-1} min^{-1}) values (Table 2) have increased with increasing temperature from 283 (±1.6) to 328 (±1.6) K, and

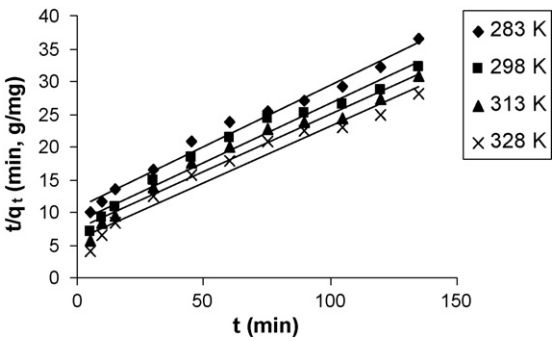

Fig. 9. The pseudo-second order plots related to the effect of temperature on adsorption kinetics of fluoride by HITMO (C_i = 25 mg L^{-1} and pH 6.40 (±0.2).

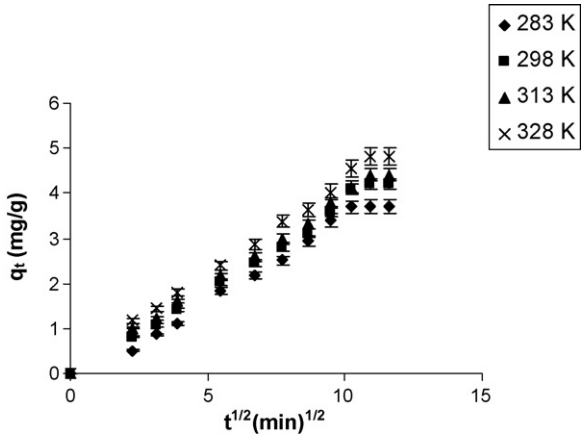

Fig. 10. The intra-particle diffusion plots related to the effect of temperatures on adsorption kinetics of fluoride by HITMO (C_i = 25 mg L^{-1} and pH 6.40 (±0.2).

the result obtained has been found to be similar to that due to Ho et al. [41].

Fig. 10 shows the plots of the time dependent adsorption capacity (q_t, mg g^{-1}) values those obtained with increase of temperature on the reactions versus the square root of the contact time ($t^{0.5}$, min$^{0.5}$) according to the Eq. (4). It has been found that the fits of the kinetic data are very good (r^2 = 0.989–0.996) and increasingly well with increasing temperature on the reaction. The initial sharp linear portion over the range of contact time has indicated that the fluoride adsorption takes place with boundary layer (film) diffusion, and the latter curved portion closer to the equilibrium time indicates the intra-particle (pore) diffusion controlled adsorption possibility of fluoride. Thus, the present adsorption kinetic reaction rate is the multi-stage controlled phenomena [13,27,44–47]. Fur-

Table 2
The kinetic parameters on fluoride adsorption on HITMO at different temperatures and pH 6.4 (±0.2). Fluoride concentration used: 25 mg L^{-1}.

Kinetic equations	Parameters	Temperature (±1.6 K)			
		283	298	313	328
Pseudo-second order	k^2 (g mg^{-1} min^{-1}) × 10^{-3}	3.37	3.82	4.19	4.89
	q_e (mg g^{-1})	5.29	5.55	5.68	5.84
	r^2	0.983	0.965	0.960	0.958
	h_0 (mg g^{-1} min^{-1})	0.095	0.117	0.135	0.167
Pseudo-first order	k_1 (min^{-1}) × 10^{-2}	3.63	2.65	2.25	2.21
	q_e (mg g^{-1})	5.54	4.80	4.35	4.61
	r^2	0.799	0.835	0.931	0.910
Intra-particle diffusion	k_{id} (g mg^{-1} min$^{-0.5}$) × 10^{-1}	3.56	3.81	3.88	4.18
	r^2	0.989	0.994	0.996	0.996

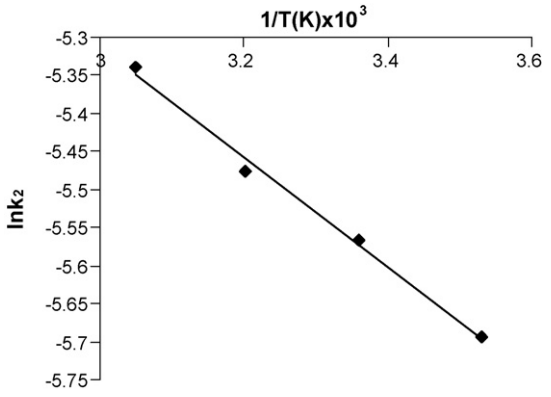

Fig. 11. The plot of $\ln k_2$ versus $1/T(\mathrm{K}) \times 10^3$ for the activation parameter for fluoride adsorption on HITMO.

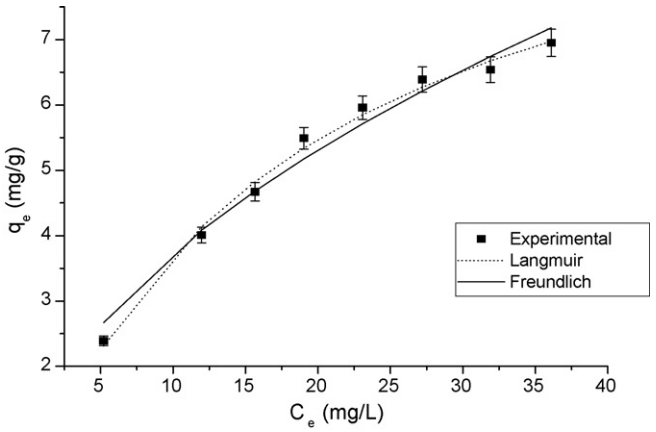

Fig. 12. The plot of equilibrium adsorption capacity versus equilibrium concentration of fluoride on HITMO at 303 (±1.6) K and at pH 6.40 (±0.2) and the non-linear data fits with the Langmuir and Freundlich isotherm models.

thermore, the calculated D_p and D_F values ($\mathrm{cm^2\ s^{-1}}$) for the studied temperature range according to the Eqs. (5) and (6), respectively, are $(1.07–1.73) \times 10^{-9}$ and $(1.59–2.81) \times 10^{-10}$, which have supported the conclusion drawn above.

3.4.3. Activation parameters

The increase in pseudo-second order rate constant (k_2) with increasing temperature may be described by the Arrhenius equation (Eq. (7)):

$$k_2 = A \exp\left(\frac{-E_a}{RT}\right) \tag{7}$$

The significance of each term present in Eq. (7) has been given in the nomenclature. Taking logarithmic of Eq. (7), the following Arrhenius type linear relationship (Eq. (8)) is obtained.

$$\ln k_2 = \ln A + \left(\frac{-E_a}{R}\right)\frac{1}{T} \tag{8}$$

The plot of $\ln k_2$ against $1/T$ shows a linear variation (Fig. 11) with a high regression coefficient ($r^2 = 0.994$) value. The intercept and slope of the plot give the temperature-independent parameter, A ($=7.2 \times 10^{-4}\ \mathrm{g\ mg^{-1}\ s^{-1}}$) and the activation energy, E_a ($=6.02\ \mathrm{kJ\ mol^{-1}}$), respectively. The result has found to be similar to that had been reported by other workers [23,49].

3.5. Isotherm modeling

Fig. 12 shows the equilibrium isotherm data as points for fluoride adsorption at pH 6.4 (± 0.2) and temperature 303 (±1.6) K on HITMO. The equilibrium data points (Fig. 12) have been analyzed by using the most widely used isotherm equations (Eqs. (9)–(12)) viz. the Langmuir [50] and the Freundlich [51] models shown below:

Langmuir isotherm:

$$q_e = \frac{\theta b C_e}{(1 + bC_e)} \quad \text{(Non-linear form)} \tag{9}$$

$$\frac{C_e}{q_e} = \frac{1}{\theta b} + \frac{C_e}{\theta} \quad \text{(Linear form)} \tag{10}$$

Frieundlich isotherm:

$$q_e = K_F C_e^{1/n} \quad \text{(Non-linear form)} \tag{11}$$

$$\log q_e = \log K_F + \frac{1}{n} \log C_e \quad \text{(Linear form)} \tag{12}$$

The symbols (Eqs. (9)–(12)) have their usual significance and given in the nomenclature.

The non-linear (plots shown in Fig. 12) and the linear (plots are not shown) analyses show the well fit of the equilibrium data with the Langmuir and the Freundlich models. The comparison of the isotherm parameters (Table 3) computed from the linear and the non-linear Langmuir and Freundlich isotherm models analyses has showed that the present data have described the Langmuir ($r^2_{(\text{non-linear})} = 0.993$, $\chi^2 = 0.0188$ and $r^2_{(\text{linear})} = 0.992$) and the Freundlich ($r^2_{(\text{non-linear})} = 0.977$, $\chi^2 = 0.0618$ and $r^2_{(\text{linear})} = 0.988$) models well. However, based on either χ^2 or r^2 value it can be concluded that the best-fit model is the Langmuir for the present case. Thus, the fluoride adsorption by HITMO has taken place with monolayer surface coverage. The monolayer adsorption capacity (θ, $\mathrm{mg\,g^{-1}}$) of HITMO for the fluoride obtained either from the linear analysis ($10.47\ \mathrm{mg\,g^{-1}}$) or from the non-linear analysis ($10.58\ \mathrm{mg\,g^{-1}}$) of present data is found to be higher than that of the pure iron(III) oxide ($7.50\ \mathrm{mg\,g^{-1}}$) [34]. The Freundlich adsorption constant (K_F, $\mathrm{L\,mg^{-1}}$) obtained, respectively, from the linear and non-linear analyses are 0.99 and 1.15. The Freundlich coefficient (n), which should have values ranging from 1 to 10, obtained from the linear and non-linear analyses are 1.79 and 1.95, respectively. This supports favorable adsorption of fluoride onto the mixed oxide. Thus, it can be suggested that the present mixed oxide is a better adsorbent in removing fluoride from water than the pure iron(III) oxide. To access the fluoride removal efficiency of the present mixed oxide, a comparison of the Langmuir monolayer capacity (θ, $\mathrm{mg\,g^{-1}}$) value of the present adsorbent has been shown (Table 4) with some other reported materials.

3.6. Thermodynamic parameters

Assuming the activity coefficient as unity at low solute concentrations (Henry's law sense), the thermodynamic parameters for the adsorption process in solution have been calculated using the following standard thermodynamic relations (Eqs. (13) and (14)):

$$\Delta G^0 = \Delta H^0 - T\Delta S^0 \tag{13}$$

and

$$\Delta G^0 = -2.303RT \log K_c \tag{14}$$

The combination of Eq. (13) with Eq. (14) gives the Eq. (15) below.

$$\log K_c = \frac{\Delta S^0}{2.303R} - \left(\frac{\Delta H^0}{2.303R}\right)\frac{1}{T} \tag{15}$$

Each term of Eqs. (13)–(15) has their usual significance and given in the nomenclature. The thermodynamic equilibrium constant, K_c

Table 3
The evaluated isotherm parameters for fluoride adsorption on HITMO at 303 (±1.6) K] and pH 6.4 (±0.2).

Isotherm model	Linear analysis parameters			Non-linear analysis parameters			
Langmuir	θ (mg g^{-1})	b (L mg^{-1})	r^2	θ (mg g^{-1})	b (L mg^{-1})	r^2	χ^2
	10.47	5.5×10^{-2}	0.992	10.58	5.36×10^{-2}	0.993	0.0188
Isotherm model	Linear analysis parameters			Non-linear analysis parameters			
Freundlich	K_F	n	r^2	K_F	n	r^2	χ^2
	0.99	1.79	0.988	1.15	1.95	0.977	0.0618

Isotherm model	Linear analysis parameters			
D–R isotherm	q_m (mol kg^{-1})	β (mol^2 kJ^{-2})	E (kJ mol^{-1})	r^2
	1.77×10^{-3}	6.1×10^{-3}	9.05	0.992

has been calculated by using equation (Eq. (16)),

$$K_c = \frac{q_e}{C_e} \tag{16}$$

where q_e/C_e is called the adsorption affinity (L g^{-1}), which is the ratio of the amount adsorbed per unit mass (q_e) to the solute concentration in solution (C_e) at equilibrium. So the above relation (Eq. (15)) can be written as (Eq. (17))

$$\log\left(\frac{q_e}{C_e}\right) = \frac{\Delta S^0}{2.303R} - \left(\frac{\Delta H^0}{2.303R}\right)\frac{1}{T} \tag{17}$$

Assuming ΔS^0 and ΔH^0 to be constant within the range of studied temperature, the values have been computed from the slope and intercept of the straight line of plots of log (q_e/C_e) versus $1/T$

Table 4
The comparative assessment of Langmuir monolayer capacity (θ, mg g^{-1}) of HITMO with some literature available data for other adsorbents.

Adsorbent	θ (mg g^{-1})	Experimental conditions	Reference
Algal biosorbent Spirogyra sp.-IO2	1.27	pH 7.0 Concentration: 5–25 mg L^{-1}	[27]
Calcined Zn/Al hydrotalcite-like compound	13.43	pH 6 Concentration: 2–60 mg L^{-1}	[28]
Hydroxyapatite	4.54	pH 6.0 and low	
Fluorspar	1.79	Concentration (2.5×10^{-5} to 6.34×10^{-2}) mol L^{-1}	
Activated quartz	1.16		[11]
Calcite	0.39		
Quartz	0.19		
Activated alumina	2.41	pH 7.0 Concentration: 2.5–14 mg L^{-1}	[30]
Acid treated spent bleaching earth	7.75	pH 3.5 Concentration: 5–20 mg L^{-1}	[13]
Iron–zirconium hybrid oxide	8.21	pH 6.8 ± 0.1 Concentration: 5–50 mg L^{-1}	[34]
Iron–aluminum mixed oxide	17.73	pH (6.9 ± 02) Concentration: 10–50 mg L^{-1}	[35]
Iron–tin mixed oxide	10.47	pH (6.4 ± 0.2) Concentration: 10–50 mg L^{-1}	Present work
$KMnO_4$-modified carbon	15.90	pH 2 Concentration: 5–20 mg L^{-1}	[23]
Plaster of Paris	0.336	pH 3–9 Concentration: 2–10 mg L^{-1}	[22]
Light weight concrete material	5.15	pH 8.9 Concentration range: probably 10–50 mg L^{-1}	[21]
Montmorillonite	3.37	pH 6 Concentration: 2–120 mg L^{-1}	[20]
Magnetic-chitosan	22.49	pH 7 Concentration: 5–40 mg L^{-1}	[19]
Quick lime	16.67	pH 6.61 Concentration: 10–50 mg L^{-1}	[18]
Laterite	0.85	pH 7.5 Concentration: 10–50 mg L^{-1}	[17]

Table 5
The thermodynamic parameters for adsorption of fluoride on HITMO.

Fluoride concentrations (mg L^{-1})	ΔH^0 (kJ mol^{-1})	ΔS^0 (J mol^{-1} K^{-1})	ΔG^0 (kJ mol^{-1}) at studied temperatures (±1.6 K)			
			283	298	313	328
10.0	4.79	8.72	2.32	2.19	2.06	1.93
25.0	10.79	24.17	4.04	3.67	3.31	2.95

(Fig. 13), and ΔG^0, the free energy change for the reaction, at various temperatures has also been calculated by using the Eq. (13). The plots have showed good linearity with very good regression coefficients (r^2 = 0.992 and 0.993). The thermodynamic parameters computed for the present case in the studied solute concentrations (10.0 and 25.0 mg L^{-1}) are given in Table 5. The positive ΔH^0 (kJ mol^{-1}) values have indicated the endothermic process of fluoride adsorption on HITMO. The positive entropy changes (ΔS^0, J mol^{-1} K^{-1}) obtained (+8.72 and +24.17) for the present system for 10.0 and 25.0 mg L^{-1} of fluoride solutions indicate the increase of entropy for the adsorption reaction. This is presumably for the increase in number of species at the solid–liquid interface due to the release of (i) aqua molecules and (ii) hydroxide ion when the solvated fluoride ion is adsorbed from the aqueous solution by the solid. The positive ΔG^0 (kJ mol^{-1}) values (Table 5) indicate the non-spontaneous nature of fluoride adsorption reaction with HITMO and, that has governed with the gain of energy from surroundings [23,49].

3.7. Energy of adsorption

The equilibrium data shown as points in Fig. 12 have been analyzed by the Dubinin–Radushkevick (D–R) equation (Eq. (18)) [23,49,52] for evaluating the average energy of adsorption.

$$\ln q_e = \ln q_m - \beta\varepsilon^2 \quad (18)$$

$$\varepsilon = RT \ln\left(1 + \frac{1}{C_e}\right) \quad (19)$$

Nomenclature shows the significance of the terms present in the Eqs. (18) and (19).

The q_m (mol kg^{-1}) and β (mol^2 kJ^{-2}) values are evaluated from the intercepts and slopes of the plots of $\ln q_e$ versus ε^2 (Fig. 14). The mean free energy of adsorption (E_{DR}) is the free energy change when one mole of a solute is transferred to the surface of the adsorbent from infinity in the solution [52], and that has been calculated by the equation (Eq. (20))

$$E_{DR} = \frac{1}{(2\beta)^{1/2}} \quad (20)$$

The magnitude of E_{DR} (kJ mol^{-1}) is useful for estimating the type of adsorption reaction, and if it ranged between 8.0 and 16.0 the adsorption should be taken place by ion exchange reaction [23,49]. The D–R parameters and mean free energies evaluated are shown in Table 3. In the present case, the E_{DR} value obtained (9.05 kJ mol^{-1}) is ranged in 8.0–16.0 kJ mol^{-1}, which indicates anion-exchange mechanism for the adsorption of fluoride onto HITMO.

3.8. Effect of some other ions on fluoride removal

The adverse effect of some ions viz. calcium, magnesium, chloride, nitrate, sulfate, phosphate and bicarbonate had been tested on fluoride removal by HITMO. The concentration chosen for the ions was the level that had been encountered commonly in the ground water. The results obtained show that the tested ions have no adverse influence on the fluoride removal excepting bicarbonate ion. The fluoride adsorption capacity of HITMO has reduced from 4.70 mg g^{-1} (zero bicarbonate) to 3.80 mg g^{-1} (400 mg bicarbonate L^{-1}) from the fluoride solution of concentration 25.0 mg L^{-1}.

3.9. Desorption study

The pH effect on fluoride adsorption by HITMO showed (Fig. 3) that the fluoride adsorption capacity of HITMO is very low in alkaline pH. Based on this, batch desorption tests of fluoride from the solid surface were conducted by different solutions of pH ranged in 10.0–14.0. It has been found that the solution of pH 13 (0.1 M NaOH) is an optimum one which desorbs ~75% of the adsorbed fluoride when 25 mL fractions of pH 13 solution per g fluoride-rich HITMO (F^- content: 10.0 mg g^{-1}) in five times are added and agitated.

4. Removal of fluoride from natural water

Fig. 15 shows the results on the fluoride removal from the natural ground water sample (added fluoride concentration: 2.97 mg L^{-1}). It has been found that the concentration of fluoride reduces with increasing the solid material, HITMO, dose (in g L^{-1}) from 0.5, 1.0, 1.5, 2.0, 2.5 and 3.0. The results (Fig. 15) show when HITMO dose was

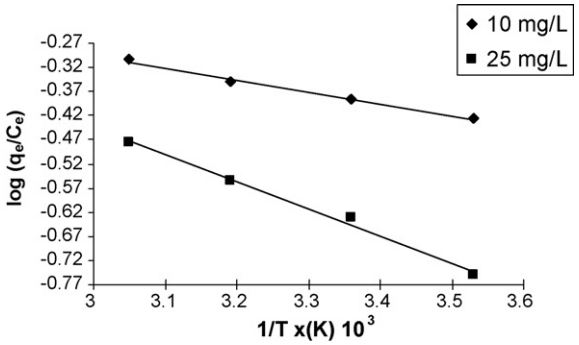

Fig. 13. The plot of $\log(q_e/C_e)$ against $1/T(K) \times 10^3$ for thermodynamic parameters.

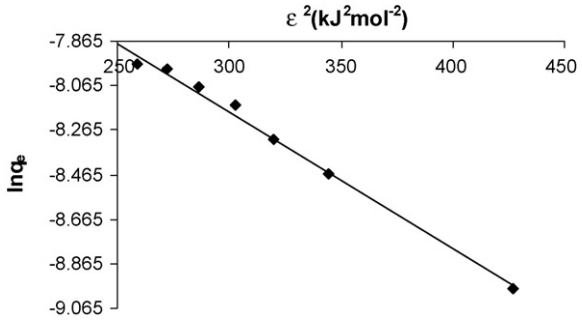

Fig. 14. The Dubinin–Raduskevich (D–R) isotherm plot of the equilibrium data for the adsorption energy.

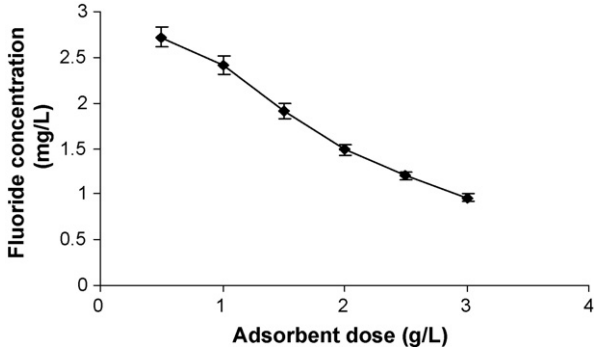

Fig. 15. The batch fluoride removal with varying HITMO dose per litre of the natural water sample.

2.0 g L^{-1}, the fluoride concentration has decreased to 1.49 mg L^{-1}, which is below the toxic level of fluoride concentration in drinking water for the cooler climatic countries and, when the dose used was 2.5 g L^{-1} that goes to below 1.0 mg L^{-1}, the permissible level for hotter climatic countries (WHO).

5. Conclusion

The HITMO has been synthesized by a simple method and the material is amorphous with irregular surface morphology. The pHzpc is 6.5 (±0.3) for this material. The fluoride adsorption capacity decreases with increasing initial solution pH (pH_i) from 3.0 to 5.0, and remains nearly same up to pH_i 7.5. The kinetic data describes the pseudo-second order model very well. The rate-limiting step is multiple-stage controlled. The equilibrium data describes the Langmuir isotherm well, and the monolayer adsorption capacity is ~10.50 mg g^{-1}. The adsorption energy (9.05 kJ mol^{-1}) evaluated suggests the ion exchange mechanism. The fluoride adsorption reaction with HITMO is endothermic and non-spontaneous process. The high bicarbonate shows adverse influence on fluoride removal by HITMO. The solution of pH 13.0 (25 mL × 5 times) can regenerate 1.0 g fluoride-rich material up to a level of ~75%. Two-gram material per liter of natural water (2.97 mg F^- L^{-1}) can reduce fluoride level below 1.5 mg L^{-1} in batch process.

Acknowledgements

The authors acknowledge sincerely to the Ministry of Water Resources and Central Groundwater Board for the financial support, and also grateful to the Principal, Presidency College and the Head, Department of Chemistry, Presidency College, Kolkata, India for laboratory facilities.

References

[1] A.K. Susheela, Flurosis management programme in India, Curr. Sci. 77 (1999) 1250–1256.
[2] V.K. Saxena, S. Ahmed, Dissolution of fluoride in groundwater, Environ. Geol. 40 (2001) 1084–1087.
[3] C.L. Yang, R. Dluhy, Electrochemical generation of aluminium sorbent for fluoride adsorption, J. Hazard. Mater. B94 (2002) 239–252.
[4] E.J. Reardon, Y.A. Wang, Limestone reactor for fluoride removal from waste waters, Environ. Sci. Technol. 34 (2000) 3247–3253.
[5] Y.H. Li, S. Wang, A. Cao, D. Zhao, X. Zhang, C. Xu, Z. Luan, D. Ruan, J. Liang, D. Wu, B. Wei, Adsorption of fluoride from water by amorphous alumina supported on carbon nanotubes, Chem. Phys. Lett. 350 (2001) 412–416.
[6] M. Srimurali, A. Pragathi, J.A. Karthikeyan, Study on removal of fluoride from drinking water by adsorption onto low cost materials, Environ. Pollut. 99 (1998) 285–289.
[7] M. Yang, T. Hashimoto, N. Hoshi, H. Myoga, Fluoride removal in a fixed bed packed with granular calcite, Water Res. 33 (1999) 3395–3402.
[8] R. Piekos, S. Paslawaska, Fluoride uptake characteristic of fly ash, Fluoride 32 (1999) 14–19.
[9] A.S. Wasay, Md.J. Haron, S. Tokunaga, Adsorption of fluoride, phosphate and arsenate ions on lanthanum impregnated silica gel, Water Environ. Res. 68 (1996) 295–300.
[10] Y. Cengeloglu, E. Kir, M. Ersoz, Removal of fluoride from aqueous solution by using red mud, Sep. Purif. Technol. 28 (2002) 81–86.
[11] X. Fan, D.J. Parker, M.D. Smith, Adsorption kinetics of fluoride on low cost materials, Water Res. 37 (2003) 4929–4937.
[12] A.V. Jamode, V.S. Sapkal, V.S. Jamode, Defluoridation of water using inexpensive adsorbents, J. Ind. Inst. Sci. 84 (2004) 163–171.
[13] M. Maharamanlioglu, I. Kizilcikli, I.O. Bicer, Adsorption of fluoride from aqueous solution by acid treated spent bleaching earth, J. Fluorine Chem. 115 (2002) 41–47.
[14] Y. Zhou, C. Yu, Y. Shan, Adsorption of fluoride from aqueous solution on La^{3+}-impregnated cross-linked gelatin, Sep. Purif. Technol. 36 (2004) 89–94.
[15] X.-P. Liao, B. Shi, Adsorption of fluoride on zirconium(IV)-impregnated collagen fibre, Environ. Sci. Technol. 39 (2005) 4628–4632.
[16] N. Das, P. Pattanaik, R. Das, Defluoridation of drinking water using activated titanium rich bauxite, Colloid. Interf. Sci. 292 (2005) 1–10.
[17] M. Sarkar, A. Banerjee, P.P. Pramanik, A.R. Sarkar, Use of laterite for the removal of fluoride from contaminated drinking water, Colloid. Interf. Sci. 302 (2006) 432–444.
[18] M. Islam, R.K. Patel, Evaluation of removal efficiency of fluoride from aqueous solution using quick-lime, J. Hazard. Mater. 143 (2007) 303–310.
[19] W. Ma, F.-Q. Ya, M. Han, R. Wang, Characteristic of equilibrium kinetics studies for the adsorption of fluoride on magnetic-chitosan particle, J. Hazard. Mater. 143 (2007) 296–302.
[20] A. Tor, Removal of fluoride from aqueous solution by using montmorillonite, Desalination 201 (2006) 267–276.
[21] E. Oguz, Equilibrium isotherms and kinetics studies for the sorption of fluoride on light weight concrete materials, Colloids Surf. A: Physicochem. Eng. Aspects 295 (2007) 258–263.
[22] V. Gopal, K.P. Elango, Equilibrium kinetics and thermodynamics studies of adsorption of fluoride onto plaster of paris, J. Hazard. Mater. 141 (2007) 98–105.
[23] A.A.M. Daifullah, S.M. Yakout, S.A. Elreefy, Adsorption of fluoride in aqueous solutions using $KMnO_4$–modified activated carbon derived from stem pyrolysis of rich straw, J. Hazard. Mater. 147 (2007) 633–643.
[24] M. Sarkar, A. Banerjee, P.P. Pramanik, Kinetics and mechanism of fluoride removal using laterite, Ind. Eng. Chem. Res. 45 (2006) 5920–5927.
[25] S.P. Kamble, S. Jagtap, M.K. Labhsetwar, D. Thakare, S. Godfrey, S. Tevotta, S.S. Rayalu, Defluoridation of drinking water using Chitin, Chitosan and lanthanum-modified chitosan, Chem. Eng. J. 129 (2007) 173–180.
[26] S.M. Maliyekkal, A.K. Sharma, L. Philip, Manganese oxide-coated alumina: a promising sorbent for defluoridation of water, Water Res. 40 (2006) 3497–3506.
[27] S.V. Mohan, S.V. Ramanaiah, B. Rajkumar, P.N. Sarma, Removal of fluoride from aqueous phase by biosorption on to algal biosorbent spirogyra Sp.–102: sorption mechanism elucidation, J. Hazard. Mater. 141 (2007) 465–474.
[28] D.P. Das, J. Das, K. Parida, Physicochemical characterization and adsorption behavior on calcined Zn/Al hydrotalcite-like compound (HTlc) towards removal of fluoride from aqueous solution, Colloid Interf. Sci. 261 (2003) 213–220.
[29] X. Wu, Y. Zhang, X. Dou, M. Yang, Fluoride removal performance of a novel Fe-Al-Ce trimetal oxide adsorbent, Chemosphere 69 (2007) 1758–1764.
[30] S. Ghorai, K.K. Pant, Investigation on the column performance of fluoride adsorption by activated alumina in a fixed bed, Chem. Eng. J. 98 (2004) 165–173.
[31] I. Abe, S. Iwasaki, T. Tokimoto, N. Kawasaki, T. Nakamura, S. Tanada, Adsorption of fluoride ions onto carbonaceous materials, Colloid Interf. Sci. 275 (2004) 35–39.
[32] S. Dey, S. Goswami, U.C. Ghosh, Hydrous ferric oxide—a scavenger of fluoride from contaminated water, Water Air Soil Pollut. 158 (2004) 311–323.
[33] S. Goswami, S. Dey, U.C. Ghosh, Studies on Removal of fluoride by hydrated zirconium oxide, Chem. Environ. Res. 13 (2004) 117–126.
[34] K. Biswas, D. Bandhoyapadhyay, U.C. Ghosh, Adsorption kinetics of fluoride on iron(III)–zirconium(IV) hybrid oxide, Adsorption 13 (2007) 83–94.
[35] K. Biswas, S.K. Saha, U.C. Ghosh, Adsorption of fluoride from aqueous solution by a synthetic iron(III)–aluminum(III) mixed oxide, Ind. Eng. Chem. Res. 46 (2007) 5346–5356.
[36] APHA, AWWA, WEF, Standard methods for the examination of water and wastewater, in: L.S. Clesceri, A.E. Greenberg, A.D. Eaton (Eds.), 20th edn. Washington, DC, 1998; pp. 4–82.
[37] B.M. Babic, S.K. Milonjic, M.J. Polovina, B.V. Kaludierovic, Point of zero charge and intrinsic equilibrium constants of activated carbon cloth, Carbon 37 (1999) 477–481.
[38] S. Largergren, Zur theorie der sogenannten adsorption gelöster stoffe, Kungliga Svenska Vetenskapsakademiens, Handlingar 24 (1898) 1–39.
[39] Y.S. Ho, G. McKay, Kinetic model for lead(II) sorption onto peat, Adsorp. Sci. Technol. 16 (1998) 243–255.
[40] W.J. Weber Jr., J.C. Morriss, Kinetics of adsorption on carbon from solution, J. Sanit. Div. Am. Soc. Civ. Eng. 89 (1963) 31–60.
[41] Y.S. Ho, T.H. Chiang, Y.M. Hsueh, Removal of basic dye from aqueous solution using tree fern as a biosorbent, Process Biochem. 40 (2005) 119–124.

[42] E. Demirbas, M. Kobya, E. Senturk, T. Ozkan, Adsorption kinetics for the removal of chromium(VI) from aqueous solutions on the activated carbons prepared from agricultural waste, Water SA 30 (2004) 533–539.
[43] I. Uzun, Kinetics of the adsorption of reactive dyes by chitosan, Dyes Pigments 70 (2006) 76–83.
[44] V.C. Srivastava, M.M. Swamy, I.D. Mall, B. Parasad, I.M. Mishra, Adsorptive removal of phenol by bagasse fly ash activated carbon: equilibrium, kinetics and thermodynamics, Colloids Surf. A: Physicochem. Eng. Aspects 272 (2006) 89–104.
[45] K.K. Singh, R. Rastigo, S.H. Hasan, Removal of Cr(VI) from waste water using rice bran, Colloid Interf. Sci. 290 (2005) 61–68.
[46] V.K. Kumar, V. Ramamurthi, S. Sivanesan, Modeling the mechanism involved during the sorption of methylene blue onto fly ash, Colloid Interf. Sci. 284 (2005) 14–21.
[47] T.S. Sing, K.K. Pant, Equilibrium, kinetics and thermodynamics studies for adsorption of As(III) on activated alumina, Sep. Purif. Technol. 36 (2004) 139–147.
[48] F. Helfferich, Ion Exchange, McGraw-Hill, New York, 1962.
[49] A. Ozcan, E.M. Oncu, S. Ozcan, Kinetics, isotherm and thermodynamic studies of adsorption of acid blue 193 from aqueous solutions onto natural sepiolite, Colloids Surf. A: Physicochem. Eng. Aspects 277 (2006) 90–97.
[50] I. Langmuir, The constitution and fundamental properties of solids and liquids. Part I. Solids, J. Am. Chem. Soc. 38 (1916) 2221–2295.
[51] H.M.F. Freundlich, Over the adsorption in solution, Zeitsschrift fur (J. Phys. Chem.) 57 (1905) 385–470.
[52] M.M. Dubinin, L.V. Radushkevich, Proc. Acad. Sci. U.S.S.R. Phys. Chem. Sect. 55 (1947) 331.